VISUALIZATION OF SUBMERGED CAVITATING JET BEHIND THE MICRO ORIFICE

R. OLŠIAK[1,c], M. MLKVIK[1], B. KNÍŽAT[1]

[1]Slovak University of Technology, Institute of Chemical and hydraulic machines and equipment, Bratislava, Slovakia

[c]Corresponding author: Tel.: +421 917825279 ; Email: robert.olsiak@stuba.sk

KEYWORDS:
Main subjects: cavitating jet impinging, flow visualization
Fluid: cavitating micro jet in water
Visualization method(s): high speed photography, spark light
Other keywords: micro orifice, video data processing

ABSTRACT: Visualization of a cavitating jet in fluids is a powerful tool for an analysis of cavitation effects on solid surfaces of mechanical parts of hydraulic components. Results of visualization of a cavitating jet behind a submerged micro orifice are presented in this paper. Generally, it may be stated, that observed jet is highly non-stationary in a time domain. Its shape and structure is strictly dependent on a distance from the output of the micro orifice. Visualization method used in described experiments is based on an acquisition of digital images (video sequences) via high speed digital video camera. Minimum exposition time of the camera is in order of 10^0 microseconds, which is not satisfactory for purposes of cavitating micro jet visualization. Thus, a spark lamp light source was used during the experiments. This light source generates flashes with 10^1 ns duration. This illumination time allows us to remove motion blur from the images. The results of experiments presented in the paper were obtained at different hydraulic conditions of the jet (defined by a cavitation number) and different test apparatus configurations: light source parameters, high speed digital camera set up.

Introduction

The visualization, as an experimental method in the field of the cavitation research, is used for a long time. The results of experimental works in cavitation visualization are presented in Brennen [1]. These works were realized on the physical models, which can be described as conventional. Currently the research teams are focused also on a research of the cavitation in the channels of the small scales, usually called microfluidics devices. These channels are defined by the characteristic hydraulic length in the range from 10^1 to 10^3 μm. The authors of these research works are primary focused on the research of the cavitation bubbles creation in the microfluidics devices [2], [4], and they use the flow visualization as a research method. The goal of these works is to determine the conditions of the cavitation inception, which allow us to optimize the geometry of the microfluidics cavitation devices. The results are also suitable for determination of the materials resistive against cavitation erosion. Presented paper is oriented on the research of the supercavitation cloud behind a micro-orifice. One of the goals is the optimization of the geometry of the orifices where the parameter of the optimization is the destructive effect of the cavitation cloud on the solid surface. The utilization of the cavitation for solid surface destruction is an alternative for the usage of the water jet technology [8].

Analysis of flow

A flow through an orifice is defined by the Bernoulli's theorem:

$$\frac{p_1 - p_2}{\rho} = C_v^{-2} \frac{v_2^2}{2} \qquad (1)$$

where p_1 is an upstream pressure, p_2 is a downstream pressure and C_v is a velocity coefficient. Cavitation regime of flow is characterized by a cavitation number:

$$\sigma = \frac{p_2 - p_v}{\frac{v_2^2}{2}\rho} \tag{2}$$

where σ is the cavitation number, ρ is a density, and v_2 is the velocity at the orifice exit.

After combinig equations (1) and (2), we obtain:

$$\frac{C_v^{-2}}{\sigma} = \frac{p_1 - p_2}{p_2 - p_v} \tag{3}$$

Assuming that C_v^{-2} is approximately constant, the relation between σ^{-1} and $\frac{p_1 - p_2}{p_2 - p_v}$ is linear.

Development of cavitation is dependent on a value of the cavitation number. Intensity of cavitation grows with decreasing cavitation number. On the base of the value of the cavitation number the flow may be classified as follows:

1. Non-cavitating flow at higher values of σ
2. Incipient cavitation, when cavitation cloud collapses inside the orifice opening.
3. Supercavitation at low values of σ, when the cavitation cloud collapses behind the orifice exit [4].

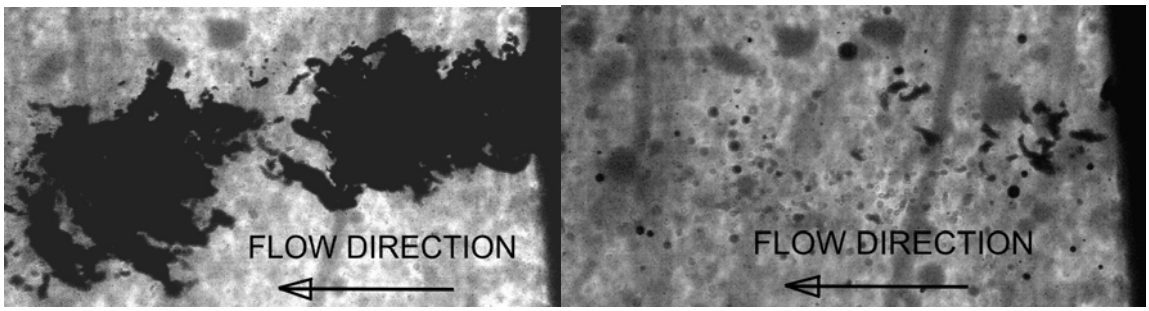

Fig. **1** - Typical flow patterns of the cavitation cloud (left) σ=0,053 (supercavitation), (right) σ=0,169. Flow velocity at the orifice exit is 59 m/s.

The goal of our work was a flow visualisation at very low cavitation numbers at extremly developed supercavitation. In the **Fig**. **1** is an example of a supercavitating flow behind a microorifice obtained during our experiments. The figure shows the influence of magnitude of the cavitation number.

When the supercavitating cloud collapses on the obstacle placed at certain distance from the orifice, another flow pattern may be observed. In our experiments we investigated this case of flow with a perpendicular obstacle placed in different distances from the orifice.

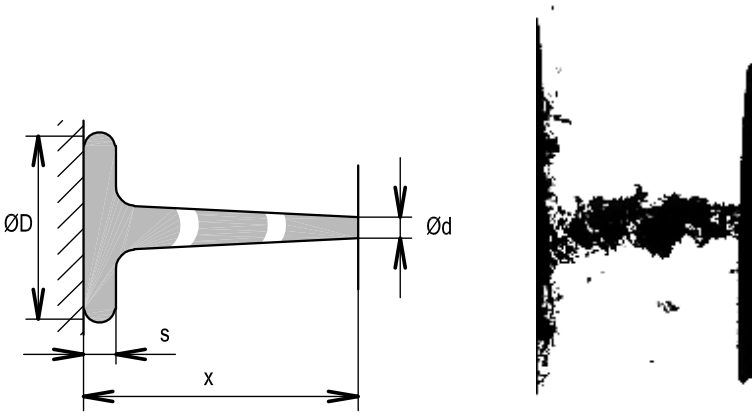

Fig. **2** – Supercavitation behind a microorifice – cavitation cloud collapses on the perpendicular wall. Left – geometrical parameters, right – snapshot of flow for orifice diameter d=0,58 mm and cavitation number σ=0,095.

In the **Fig. 2** is an example of the cavitating cloud collapse on a smooth perpendicular wall. The flow in the figure is in a supercavitating regime, an orifice opening is d and a distance from the obstacle is "x". The cloud splits and collapses at a diameter D. The cloud thickness is "a". In the **Fig**. 2 right is a snapshot of flow made in our experiments. The diameter D corresponds with the region affected by a cavitation erosion.

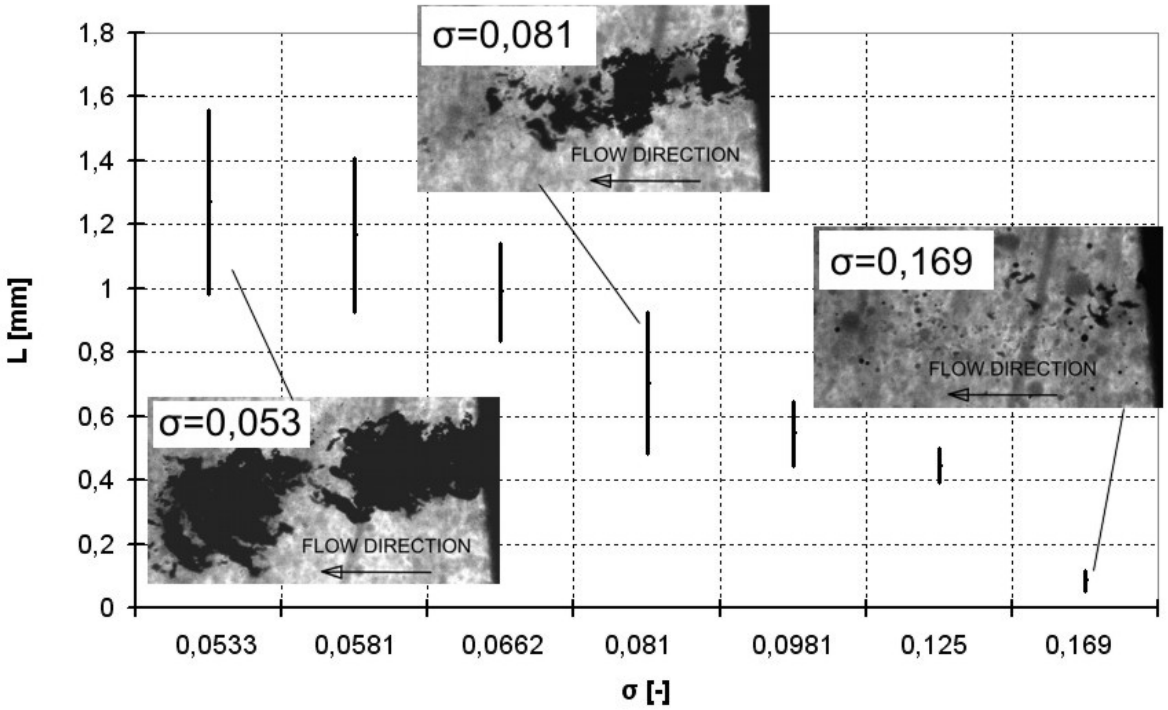

Fig. **3** – Supercavitation behind a microorifice – varying cloud length [5].

In the **Fig**. **3** is depicted the length (L) of the cavitation cloud behind a micro orifice. It is clear, that the length (L) is dependent on the cavitation number. Beside this, the L is varying in time in a certain range as it follows from the figure. The frequency of the length change is relatively high and is also dependent on the cavitation number.

It may be stated that the flow of the cavitation cloud is characterized by high velocities (up to 100 m/s) and by considerable unsteadiness. These facts influence the vizualisation methodology and make demands on the test apparatus.

Set up of experimental rig

Experimental system is composed of three major subsystems. The first one is a hydraulic circuit with a discharge nozzle (A1 – A4, B1 – B3, C1 – C2, D1 – D3, **Fig. 5**). The second one is a system for data acquisition and data processing, in common called DAQ system (a1 – a2, **Fig. 4**). The last subsystem is a visualization subsystem for images or video sequences recording, composed of two components: a high speed video camera (b1, **Fig. 4**), and a pulse light source with a high-frequency repetition (c1 – c2, Fig. 4). All of the subsystems are assembled of more partial systems and particular components, so the test rig is a relatively complicated technical equipment. The block diagram introducing the test rig is in the Fig. 4. Functions and parameters of assembled subsystems and components have fundamental influence on an application field as well as on a quality and quantity of the experimental data. They will be discussed in next sections of the article.

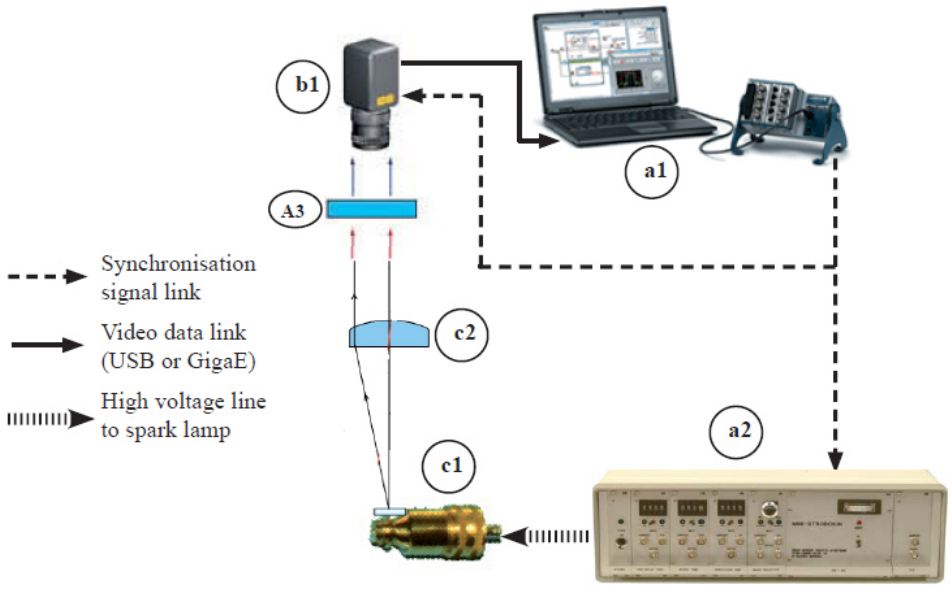

Fig. 4 Block diagram of the test rig for cavitating micro jets visualization

Specification of test rig components

The hydraulic circuit contains a discharge nozzle in a special hydraulic chamber A3. This circuit is powered by a high pressure pump station A2. Used pump is a triple piston pump, powered by AC motor controlled by a frequency charger. This station also contains an accumulator A4 for an elimination of pressure pulses. Back pressure in the test chamber A3 is equal to the pressure in a vacuum recipient B2. The pressure in the vacuum recipient B2 is reached by a vacuum pump station B1. The vacuum pump station B1 is a compact unit based on a small water ring vacuum pump powered by DC motor equipped with PWM regulator for speed control. A return line of the experimental system drains the test liquid to tank A1. This line contains also the heat exchanger C2 (for a temperature control of the test liquid). Pressurized air line D1 – D3 is designed for a stabilization of a light source parameter c1. Detailed hydraulic and mechanical scheme of the test rig is in the **Fig. 5**.

DAQ & Control Unit (**Fig**. **4**. signed a1) is used for measurements of physical parameters, transmission, archiving and manipulation of non-visual data. The system is built-in as a Power Workstation (inside INTEL Xeon processor) added on PCI or PCI-e DAQ with Control card respectively. For observation of the cavitation (bubbles or clouds) the vision system is necessary. The vision system is built-up of three subsystems. The first one: digital imaging subsystem b1 intended for video data capturing and transferring to DAQ system. The second one: optical subsystem c2 intended for transport of the optical data (optical images) to the vision subsystem. The third one: illumination subsystem c1 intended for illumination of examined phenomenon.

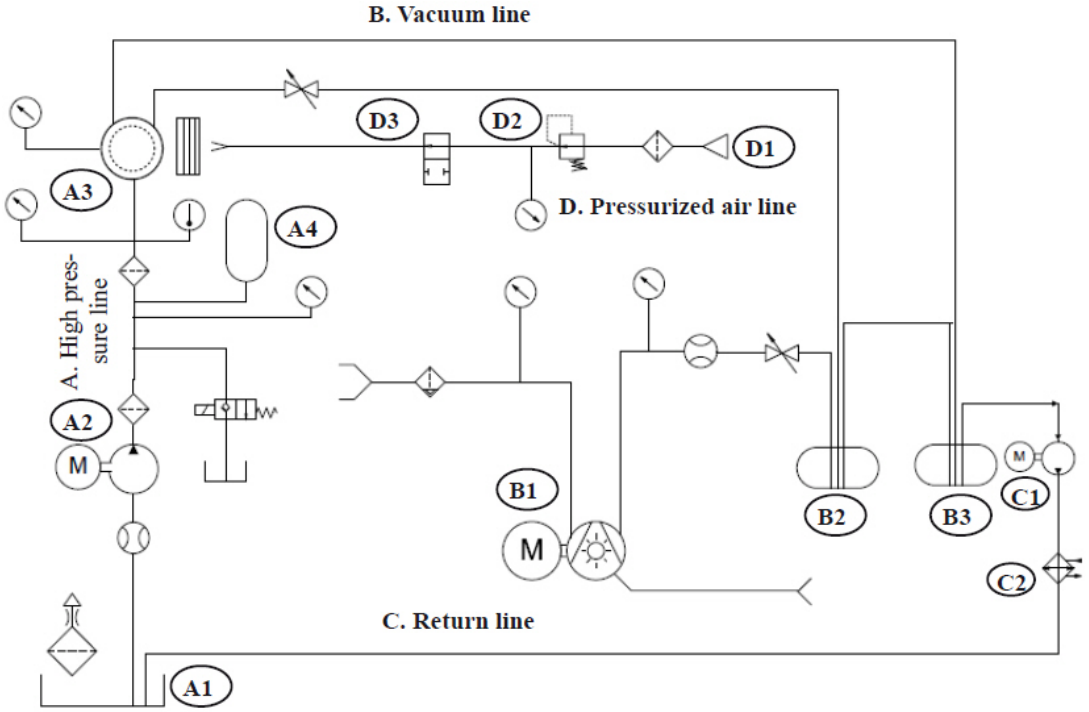

Fig. 5 Scheme of the test rig

For the purpose of digital images recording a High speed digital video camera is used. It is a monochromatic digital camera RedLake Y3 containing CMOS video chip with very low inter-frame time (less than 100 ns in double rate mode). The digital camera has 4 GB video memory and digital communication links USB 2.0 or Giga Ethernet. The optical subsystem c2 is intended for a transport of the optical data (optical image) to the vision subsystem, in this case is used NIKON 50 f 0.98 objective with optical condenser. The illumination subsystem c1, is intended for illumination of examined phenomenon. NANOLITE flash lamp with very low flash duration, typically 8 ns, is used for this application. The lamp is a source of cold white light with an extreme intensity which requires Ministrobokin flash driver. It is the high repetition lamp (up to 20 kHz) with a high voltage pulse generator, synchronized and triggered via analog TTL technology.

Numerical analysis of the cavitating flow

Measured experimental data were used as the inputs for a numerical simulation of the cavitating flows. The goal of the simulation is a comparison of the results obtained with the Zwart-Gerber cavitation model and the Singhal full cavitation model with the results of experiments.

The chosen criteria for comparison of the simulations results are used:

- Pressure loss of the analyzed jet in different flow rates
- The distribution of the vapor in the domain and the non-stationary behavior of the cavitation cloud

Computational domain and the grid

The interior of the test chamber for experiments with cavitating flows (Lichterovicz cell) has a cylindrical shape with the cavitating jet and a specimen for measurements of erosion effects placed on the one axis (**Fig.7**). This is a reason why 3-dimensional problem is converted into a 2-dimensional, axisymmetric problem. The simplified geometry used for computations is figured in (**Fig. 6**).

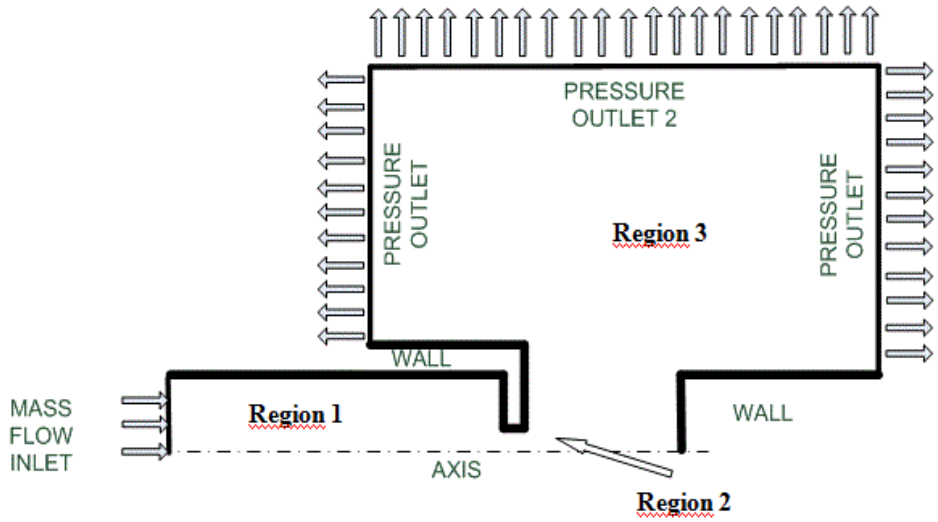

Fig.6 Used 2-D axisymmetric computational domain with boundary types

Thanks to presented simplified geometry (**Fig**. **6**), it is possible to create a map grid in the whole domain. The size of the quadrilateral elements is based on the diameter of the orifice. As can be seen from (**Fig. 6**), the domain consists of three regions of different length scales. The length scale of the first region (inlet channel) is in order of the millimeters (depends on size of the orifice). The size of the orifice itself (second region) is in order of the tens or hundreds of micrometers. The rest of the domain is in order of the centimeters. The different length scale of the domain regions is one of the reasons, why 3-dimensional computational grid has unacceptable number of the elements. The key region for the simulation is the orifice, therefore, size scale of the elements is chosen depending on the orifice diameter. Trying different sizes of the elements, we have found, that the best results are obtained when element's corner length is $d/10$. At this scale of the elements, the grid independent solution is obtained.

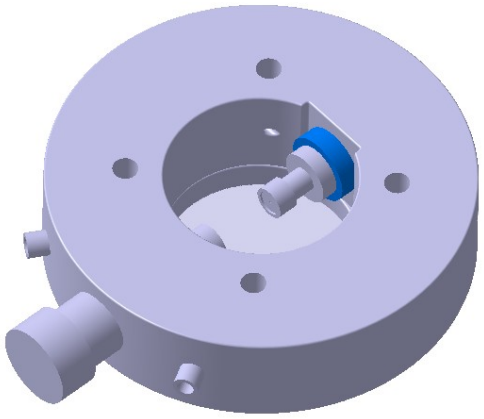

Fig.7 Real geometry of the test chamber

Physical properties of the water mixture

The fluid in the simulation is assumed as the mixture of the water in the liquid state, the water vapor and the non-dissolved air contained in the water. For the simulation purposes is the water (liquid) assumed to be non-compressible. The air and the water vapor are assumed to be ideal gases, so their density can be derived from the state equation (4).

$$\frac{p}{\rho_{air}} = z \cdot R \cdot T \tag{4}$$

The non-dissolved air strongly influences the cavitation bubbles creation, so it is important to include the volume fraction of the air to the numerical model. The value of the volume fraction can be derived from the known value of the sound speed in the water during experiments from the "IAPWS-IF97" equations (5) [7].

$$c_{mix} = c_{H_20} \cdot c_{air} \cdot \sqrt{\frac{\rho_{H_20} \cdot \rho_{air}}{\rho_{mix}}} \cdot \sqrt{\frac{1}{v_{H_20} \cdot \rho_{air} \cdot c_{air}^2 + v_{air} \cdot \rho_{H_20} \cdot c_{H_20}^2}} \tag{5}$$

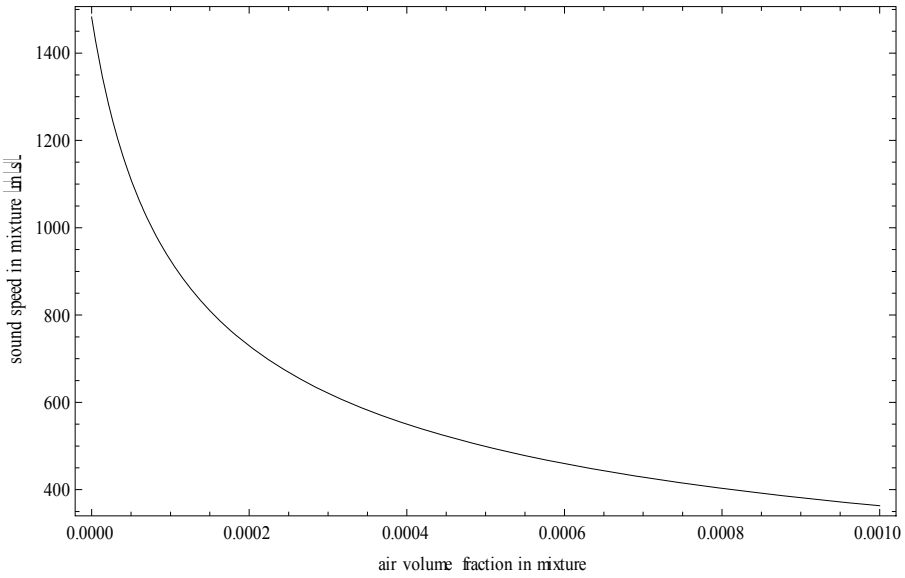

Fig 8 Sound speed in the water-air mixture depending on the non-condensable gas volume fraction for temperature 20°C

Comparison of the simulation results with the experiments

For selected cavitation numbers, there was created a high speed visual record of the cavitation cloud. The dynamic behavior and the complicated structure of the cavitation cloud can be observed on the images. The visualized structure of the cavitation cloud can be compared with simulation results. Computed distribution of the vapor phase can be seen in the (**Fig.9, 10, 11**). Both of the cavitation models give the results which are comparable with the experimental data. The Zwart-Gerber cavitation model can be assumed as accurate enough only at lower cavitation numbers, when cavitation is fully developed. For the case solved in this article is the proper accuracy achieved by the cavitation number $\sigma = 0.11$.

As can be seen on (**Fig. 12**), both of the used cavitation models are able to compute pressure loss with good accuracy. The percentage deviation from the measured data is in all cases in the range of 6%. This deviance is in accordance with the previous work in the field of the numerical analysis of the cavitating flow [6]. It can be observed that computed inlet pressure is in both cases higher than measured inlet pressure. The results obtained with Singhal cavitation model are more accurate, especially in case of higher cavitation numbers. The Singhal cavitation model is

more useful in case of flow where cavitation process is in the early stages. Increasing the deviance between solution results and the experiments with decreasing cavitation number can be explained by higher flow rates, which causes more complicated and less symmetric flow in the test chamber. Then 2-D axis symmetric solution cannot properly describe this complicated flow.

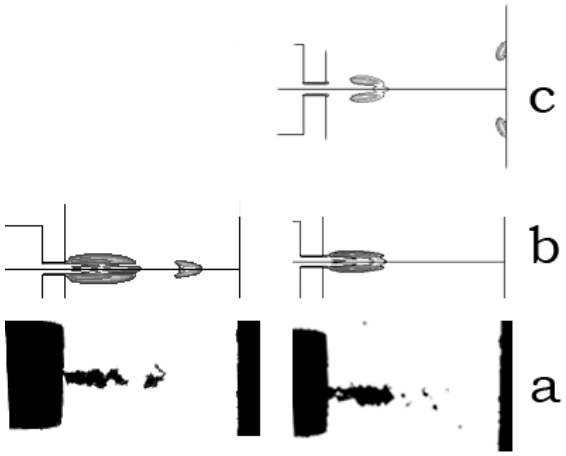

Fig. 9 Comparison of the spatial distribution of the vapor for $\sigma = 0.11$ (a-experiment, b- Singhal cavitation model, c- Zwart-Gerber cavitation model)

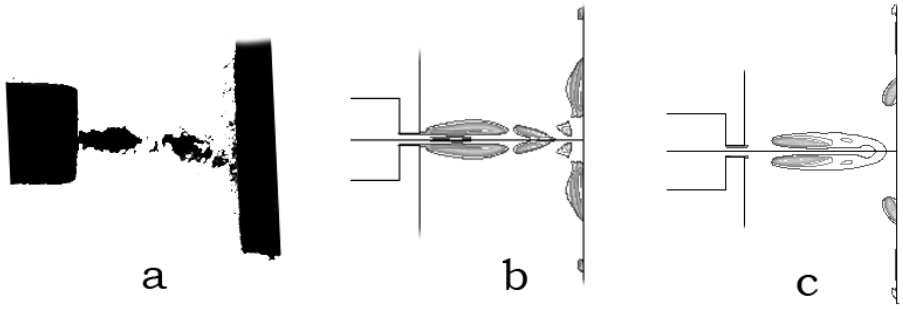

Fig. 10 Comparison of the spatial distribution of the vapor for $\sigma = 0.08$ (a - experiment, b - Singhal cavitation model, c - Zwart-Gerber cavitation model)

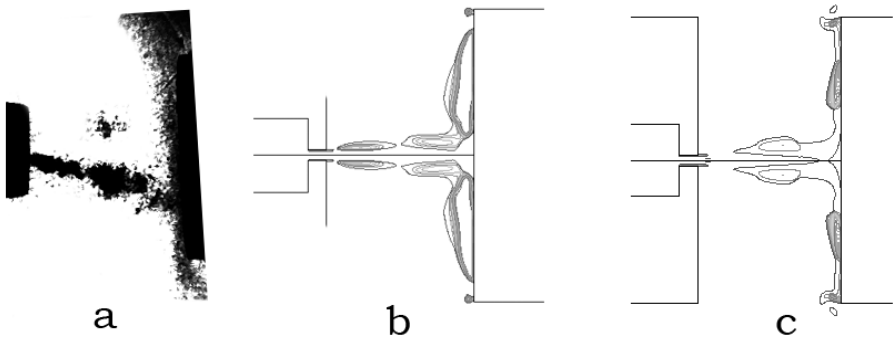

Fig. 11 Comparison of the spatial distribution of the vapor for $\sigma = 0.05$ (a - experiment, b - Singhal cavitation model, c - Zwart-Gerber cavitation model)

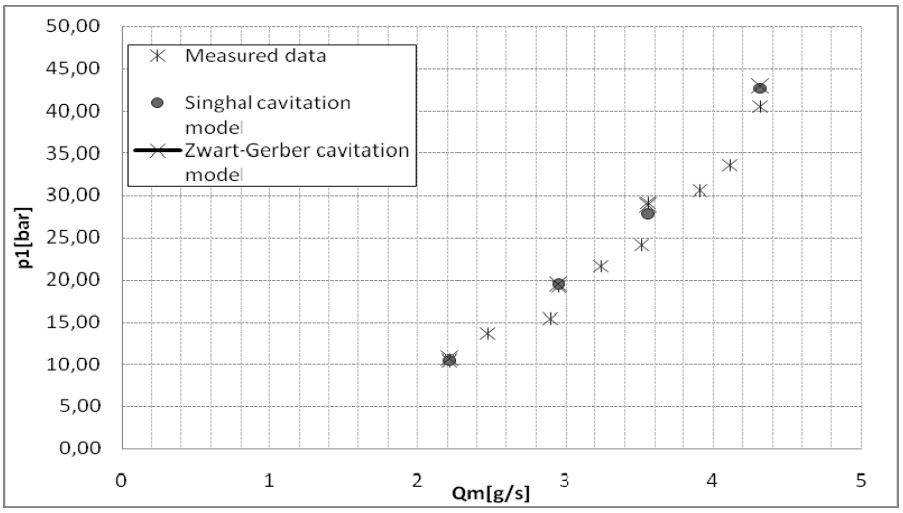

Fig. 12 Comparison of the inlet pressure simulated and measured for orifice d=0,3mm, air volume fraction included in the solution

Conclusions

In this paper are presented the results of the experimental research of the cavitation cloud behind the micro-orifice. The experiments were realized on the experimental device, where visual data and the hydraulic parameters were measured simultaneously. The qualitative dependency of the cavitation cloud shape on the cavitation number is presented (Fig. 3). For quantitative evaluation of the presented dependency, the modification of the experimental device is necessary. Also, more advanced methods of the visual data analysis must be used. The visualization results can be used for verification of the results of the CFD analysis of the cavitating flow. Two cavitation models were tested. By a comparison of the simulation results with the experimental data (Fig 8, Fig. 9, Fig. 10, Fig. 11), there can be stated, that the Singhal cavitation model provides more accurate results and it's much more suitable for the case of the early stages of the creation of the cavitation cloud.

Acknowledgement

This work was supported by the Scientific Grant Agency VEGA under contract number 1/0251/11.

References

[1] Brennen C.E.: *Cavitation and Bubble Dynamics,* New York, Oxford, Oxford University Press, 1995
[2] Mishra Ch., Peles Y.: *Development of Cavitation in Refrigerant (R-123) Flow Inside Rudimentary Microfluidic System.* Journal of microelectromechanical systems 2006, Vol. 15, No. 5, p. 1319
[3] Olšiak R.: *Experimental set up for observation of flow in channels with very small scale.* Proceedings of the XVII. AENMMTE, Bojnice, Slovakia, 2010, p. 233
[4] Chaves H., Knapp M., Kubitzek A., Obermeier F., Schneider T.: *Experimental Study of Cavitation in the Nozzle Hole of Diesel Injectors Using Transparent Nozzles*. SAE Paper 950290, March 1955.
[5] Knížat B., Olšiak R., Mlkvik M.: *Experimental Research of a Microjet Cavitation*. Experimental Fluid Mechanics 2011, Proceedings of the International Conference, November 22.-25., 2011, Jičín, Czech Republic
[6] Kozubková M.: *Matematické modely kavitace a hydraulického rázu.* VŠB- Technická Univerzita Ostrava, Ostrava 2009, ISBN 978-80-248-2043
[7] Habán V.: *Vysokofrekvenční pulsace ve vodních strojíc,* Habilitační práce. VUT v Brně, Fakulta strojního inženýrství, Brno, 2010
[8] Hutli E.A, Nedeljkovic, M. Ilic V.: *Visualization of Submerged Cavitating Jet: Part One.* Proceedings of the 16th Australasian Fluid Mechanics Conference, Crown Plaza, Gold Coast, Australia 2-7 December 2007, pages 876-880